Heavier Precipitation in Response to Longer-Lasting Tropical Cyclones and Rapid Urbanization over the Yangtze River Delta of Eastern China

LIHONG WEI,[a] XIHUI GU,[a,b,c,d,e,f] LOUISE J. SLATER,[g] YANGCHEN LAI,[h] DONGDONG KONG,[a,d] JIANYU LIU,[i] JIANFENG LI,[h] AND XIANG ZHANG[j]

[a] *Department of Atmospheric Science, School of Environmental Studies, China University of Geosciences, Wuhan, China*
[b] *Guangdong–Hong Kong Joint Laboratory for Water Security, Beijing Normal University at Zhuhai, Zhuhai, China*
[c] *State Key Laboratory of Water Resources and Hydropower Engineering Science, Wuhan University, Wuhan, China*
[d] *Centre for Severe Weather and Climate and Hydro-geological Hazards, Wuhan, China*
[e] *Hubei Key Laboratory of Yangtze Catchment Environmental Aquatic Science, School of Environmental Studies, China University of Geosciences, Wuhan, China*
[f] *State Environmental Protection Key Laboratory of Source Apportionment and Control of Aquatic Pollution, Ministry of Ecology and Environment, China*
[g] *School of Geography and the Environment, University of Oxford, Oxford, United Kingdom*
[h] *Department of Geography, Hong Kong Baptist University, Hong Kong, China*
[i] *Hubei Key Laboratory of Critical Zone Evolution, School of Geography and Information Engineering, China University of Geosciences, Wuhan, China*
[j] *National Engineering Research Center of Geographic Information System, School of Geography and Information Engineering, China University of Geosciences, Wuhan, China*

(Manuscript received 16 November 2022, in final form 8 September 2023, accepted 10 October 2023)

ABSTRACT: Precipitation induced by tropical cyclones (TCs) over cities is associated with both TC duration and urbanization; however, observational evidence of the impacts of TC duration and urbanization on precipitation in megalopolises is limited. In this study, the Yangtze River Delta (YRD) of eastern China is taken as a typical region because this region has been experiencing both rapid urbanization processes and frequent TC attacks. During 1979–2018, we find reduced translation speed and increased meandering of TCs over the YRD, resulting in increased TC duration and the proportion of TC stalling in this region. The correlation between TC duration and TC-induced precipitation amount is significant across the YRD region but is relatively weak in areas with faster urbanization expansion rates. Long-term increases in TC-induced precipitation are found in both rural and urban areas but are larger for urban areas. Urbanization plays an important role in enhancing TC-induced precipitation over urban areas of the YRD region. Areas with faster urbanization expansion rates and longer TC durations have larger TC-induced precipitation, suggesting that urban expansion and TC duration jointly amplify TC-induced precipitation. Our findings suggest that urban planners, in areas potentially affected by TCs, should consider adaptation measures to mitigate the impacts of urban rainstorms amplified by the combined effects of TCs and urbanization.

SIGNIFICANCE STATEMENT: The combined impacts of tropical cyclone (TC) duration and urbanization on precipitation have received limited attention, especially in populated urban areas. Here, we focus on the Yangtze River Delta (YRD) of eastern China, an urban agglomeration frequently impacted by TCs. We find that slowed translation and increased meandering of TCs have led to longer TC duration and stalling over the 500-km YRD buffer during 1979–2018. Significant positive correlation between TC duration and TC-induced precipitation indicates that longer-lasting TCs trigger greater precipitation. The greater TC-induced precipitation due to increased TC duration is further amplified by urban expansion.

KEYWORDS: Extreme events; Tropical cyclones; Urban meteorology

1. Introduction

Rainstorms induced by tropical cyclones (TCs) often lead to environmental disasters (Peduzzi et al. 2012; Shao et al. 2021; Woodruff et al. 2013; Q. Zhang et al. 2018; W. Zhang et al. 2018; Wang et al. 2023a, 2023b), such as flooding and waterlogging (Marsooli et al. 2019; Wang et al. 2021; Lai et al. 2021), which pose serious threats to human life and property, especially in urban areas. For example, Hurricane Harvey in 2017 brought more than 1300 mm of precipitation in five days to densely populated Houston, causing unprecedented flooding across the city (W. Zhang et al. 2018). Supertyphoon Lekima in 2019 brought exceptionally heavy precipitation over densely populated and highly urbanized areas of eastern China, causing severe flooding and affecting around 14 million people, with direct losses reaching 51 billion Chinese yuan (Shao et al. 2021).

Heavy precipitation induced by TCs is associated with TC motion characteristics (Hall and Kossin 2019; Lai et al. 2020). Generally, the slower a TC moves, the longer duration it

Corresponding authors: Xihui Gu, guxihui421@163.com; Yangchen Lai, 18481728@life.hkbu.edu.hk

DOI: 10.1175/JCLI-D-22-0854.1

travels (Hall and Kossin 2019; Liu and Wang 2020; Wang et al. 2022, 2023c). This may lead to the TC lingering in a region, leaving the region vulnerable to persistent TC-induced storms and thus greater likelihood of flooding, especially for urban areas. In urban areas, the urban heat island (UHI) effect may further amplify heavy precipitation (Yu et al. 2022; Singh et al. 2016; X. Yang et al. 2017), and impervious surfaces can also exacerbate rainstorm-flooding (Shao et al. 2019; Ress et al. 2020; Zhou et al. 2013), which can further increase TC-induced rainstorm damages. Understanding the response of TC-induced precipitation to both TC duration and urbanization in urban areas is essential to enable adaptation to future urbanization and changes in TC characteristics.

TC motion features, such as translation speed, duration, and decay rate, have changed noticeably over the past decades (Hall and Kossin 2019; Kossin 2018; Lai et al. 2020; Li and Chakraborty 2020; Song et al. 2021; Zhang et al. 2020). The translation speed of global TCs has decreased by about 10% during 1949–2016, and this slowdown is the most pronounced over the western North Pacific (WNP), with a drop of 21% (Kossin 2018, 2019). The translation speed of global landfalling TCs also showed a downward trend (Kossin 2018), and the translation speed of TCs over the coast of China has decreased by about 11% from 1961 to 2017 (Lai et al. 2020). Additionally, previous studies showed that the decay in intensity of landfalling TCs has slowed during the past decades in the North Atlantic (Zhu and Collins 2021; Li and Chakraborty 2020) and the WNP (Song et al. 2021). Once TCs make landfall, both the reduced translation speed and the decrease in the rate of decay may result in increased TC duration over land. For example, Chen et al. (2011) found that overland TC duration significantly increased over China during 1975–2009. As mentioned above, changes in TC motion features have been paid a lot of attention; however, just a few studies have quantified the responses of TC-induced precipitation to these changes in TC motion features (Hall and Kossin 2019; Lai et al. 2020). For example, the total amount of TC-induced precipitation is proportional to TC duration and the inverse of TC translation speed (Hall and Kossin 2019; Lai et al. 2020): Lai et al. (2020) reported that slow-moving TCs are more prone to deliver high total precipitation in coastal areas of China during 1961–2017, and Hall and Kossin (2019) found that there is a clear increase in accumulated rainfall per TC with residence time over the North American coast during 1948–2017. To our knowledge, observational evidence on the response of TC-induced precipitation over various regions is still limited, especially over densely populated and urbanized regions.

Heavy precipitation in cities is usually intensified by urbanization, which is associated with thermodynamic and dynamic responses of atmosphere to urbanization (Gu et al. 2019; Li et al. 2020; Wang et al. 2018; P. Yang et al. 2017). Specifically, urban impacts on heavy precipitation occur by the following possible mechanisms (Qian et al. 2022; Ao et al. 2022; Yu et al. 2022): 1) enhancement of increasing surface roughness on moisture convergence; 2) impacts of UHI effects on the urban boundary layer and atmospheric circulation; 3) impacts of urban aerosols on cloud condensation nuclei; and 4) impacts of the urban canopy on the bifurcation of precipitation systems. The urban effects on heavy precipitation and TC-induced precipitation have been shown by observations and simulations in many metropolises, including the Yangtze River Delta (YRD) of eastern China, an urban agglomeration frequently impacted by TCs. For example, Yu et al. (2022) found that urbanization led to an increase in 26.4% of heavy precipitation in the YRD urban areas during 1961–2019; Jiang et al. (2020) found increased trends in the frequency of occurrence and amount of both non-TC and TC-induced summertime extreme hourly precipitation in the YRD urban areas during 1975–2018. For TC-induced precipitation, numerical simulations carried out for one TC suggested that urbanization amplifies Hurricane Harvey–induced heavy precipitation over Houston, Texas, in 2017 (W. Zhang et al. 2018). However, no study to our knowledge has yet analyzed the impact of urbanization on long-term changes in TC-induced precipitation.

The YRD urban agglomeration of China includes 26 central cities within the provinces of Jiangsu, Zhejiang, and Anhui, as well as Shanghai city. It is one of the most densely populated and urbanized regions in the world, is home to about 225 million people, and contributes about 25% of the national GDP in 2019. Due to its proximity to the WNP, it is also one of the areas most frequently impacted by TC-related disasters (Zhou et al. 2022; Xu et al. 2013; Xu and Du 2015). Therefore, in this study, taking the YRD region as an example, the following questions are addressed:

- Have the characteristics (e.g., translation speed and duration) of TCs affecting the YRD region changed during recent decades?
- If yes, how have these changes in TC characteristics affected TC-induced precipitation over the YRD region?
- How does urbanization affect the long-term changes of TC-induced precipitation?

2. Data

a. Gridded precipitation data

Based on remote sensing products, reanalysis datasets, and in situ observations, Yang and He (2019) developed the China meteorological forcing dataset (CMFD) with a temporal resolution of 3 h and a spatial resolution of 0.1° × 0.1° during 1979–2018. The precision of this dataset is better than satellite data and the existing international reanalysis data and is almost as good as meteorological observational data (Yang and He 2019; Yang et al. 2010; He et al. 2020). The CMFD includes 2-m air temperature, surface pressure, specific humidity, precipitation rate, and other variables and has been widely used in climate-related studies in China (Chen et al. 2020; He et al. 2021; Ren et al. 2018; Su et al. 2019; B. Wang et al. 2020; S. Wang et al. 2020), due to its temporal continuity and consistency in quality. This dataset was also used to analyze urbanization effects on extreme precipitation. For example, based on the CMFD, Su et al. (2019) found larger upward trends of extreme precipitation in urban areas of South China

during the presummer season of 1979–2015 than in rural areas.

b. Tropical cyclone best track data

The TC best track dataset is obtained from the International Best Track Archive for Climate Stewardship (IBTrACS) version 4.0 (Knapp et al. 2010). The IBTrACS merges multiple TC datasets from various agencies (such as the China Meteorological Administration, the Regional Specialized Meteorological Center Tokyo–Typhoon Center of the Japan Meteorological Agency, the Joint Typhoon Warning Center, and the Hong Kong Observatory) into a global and uniform TC database. Attributions of TC tracks (such as translation direction, and latitude and longitude of TC centers) from these agencies are revised, merged, and maintained by an algorithm in IBTrACS. These attribution values are interpolated from the 6-hourly TC tracks into 3-hourly ones. The temporal resolution of 3 h for the IBTrACS dataset is in line with that of the CMFD. The IBTrACS dataset has been collated and validated and hence widely used for TC-related studies (Daloz and Camargo 2018; Kossin 2018; Yamaguchi et al. 2020; Zhang et al. 2020). However, since global satellite observations of TCs have only become available since 1967, there are serious systematic biases in the pre-1967 TC data (Kang and Elsner 2012; Kossin et al. 2013; Landsea et al. 2006, 2010). Considering the homogeneity of TC tracks and the record period of the CMFD, we set the analysis period as 1979–2018 in this study.

c. Land use/land cover data

The land use/land cover (LULC) data used in this study were produced by Xu et al. (2020), with a spatiotemporal resolution of 30 m and an annual scale over China during 1980–2015. The authors integrated high temporal resolution and coarse spatial resolution satellite images with the 5-yearly 30-m China Land Use Database to generate the LULC dataset. The LULC dataset includes 11 land use types, with the built-up type (including settlement, factory, quarry, mining, transportation, and airport) representing urban areas. The quality assessment results show that this LULC dataset performs well in all types of LULC change detection (Xu et al. 2020).

3. Methods

a. Definition of TC motion indices

Previous studies have indicated that TC-induced precipitation is usually within a 500-km radius around the TC centers (Jiang and Zipser 2010; Khouakhi et al. 2017; Knight and Davis 2009; Q. Zhang et al. 2018). Therefore, we build a 500-km buffer around the YRD (Fig. 1a) and consider that TCs passing through this buffer could trigger precipitation in the YRD region. We identify a total of 123 TCs crossing the buffer during 1979–2018 and use their tracks to analyze the motion features of TCs (Figs. 1a,d–f).

Each of the 123 TCs consists of multiple 3-h segments (i.e., 3-h intervals between each two neighboring positions of a TC). For each segment, the TC translation speed is its length along a circle arc divided by its duration (i.e., 3 h); the TC angular deviation is the angle between its displacement vector ($\mathbf{v}_1$) and the next ($\mathbf{v}_2$), i.e., $\cos^{-1}(\mathbf{v}_1 \cdot \mathbf{v}_2/|\mathbf{v}_1||\mathbf{v}_2|)$ (Li and Chakraborty 2020). Thus, each TC segment has three attributes: translation speed, angular deviation, and duration. For each TC segment, if either one or both of its two positions lie over the 500-km YRD buffer, this segment is identified as a valid segment. We average the corresponding attributes of all valid segments of a TC to obtain its translation speed and angular deviation, and we sum the duration of all valid segments of a TC to obtain its duration.

b. Identification of TC-induced precipitation

TC-induced precipitation is usually identified as precipitation events located within an effective radius (e.g., 500 km) of the TC centers during a time window (e.g., ±1 day) (Jiang and Zipser 2010; Khouakhi et al. 2017; Knight and Davis 2009; Q. Zhang et al. 2018). This identification approach assumes that all precipitation within the given radius of TC centers during the given time window is TC-induced. However, TC intensity varies with time, and the TC-induced precipitation shield is irregular in space (Liu and Wang 2020; Ren et al. 2006, 2007).

To solve the above issues, Ren et al. (2006, 2007) developed an objective synoptic analysis technique (OSAT) to separate TC-induced precipitation from daily precipitation. The OSAT can identify precipitation induced by single TC, double TCs, and TCs in conjunction with other weather systems. In the OSAT, all potential precipitation centers are first filtered out, and precipitation belts associated with these centers are then identified. The distance function (linked to TC intensity) between precipitation belts and TC centers is built to identify TC-induced precipitation belts. The details of the OSAT can be found in Ren et al. (2006, 2007).

Compared with using daily precipitation, we employ 3-h precipitation data from the CMFD to improve the precision of detection of TC-induced precipitation events. Total annual TC-induced precipitation is counted for each grid of the YRD region during 1979–2018, and their climatological means (1979–2018) are shown in Fig. 1b. The climatological mean of annual total TC-induced precipitation gradually decreases from the southeastern to the northwestern YRD. Both the spatial distribution and magnitude of annual total TC-induced precipitation are consistent with the values shown in Yang (2019). The southern YRD region is often affected by TCs and TC-induced precipitation, and the northwestward prevailing tracks usually bring precipitation on the southwest side of their moving tracks (i.e., the southern YRD region). In our study, the selected 123 TCs are dominated by the northwestward prevailing track (Fig. 1a), and the largest TC-induced precipitation amounts indeed occur in the southern YRD region (Fig. 1b). However, the most urbanized areas over YRD are located in the central-northern YRD region (Fig. 1c) with relatively small TC-induced precipitation amounts. It suggests that the amounts and spatial distributions of TC-induced precipitation are mainly determined by TCs.

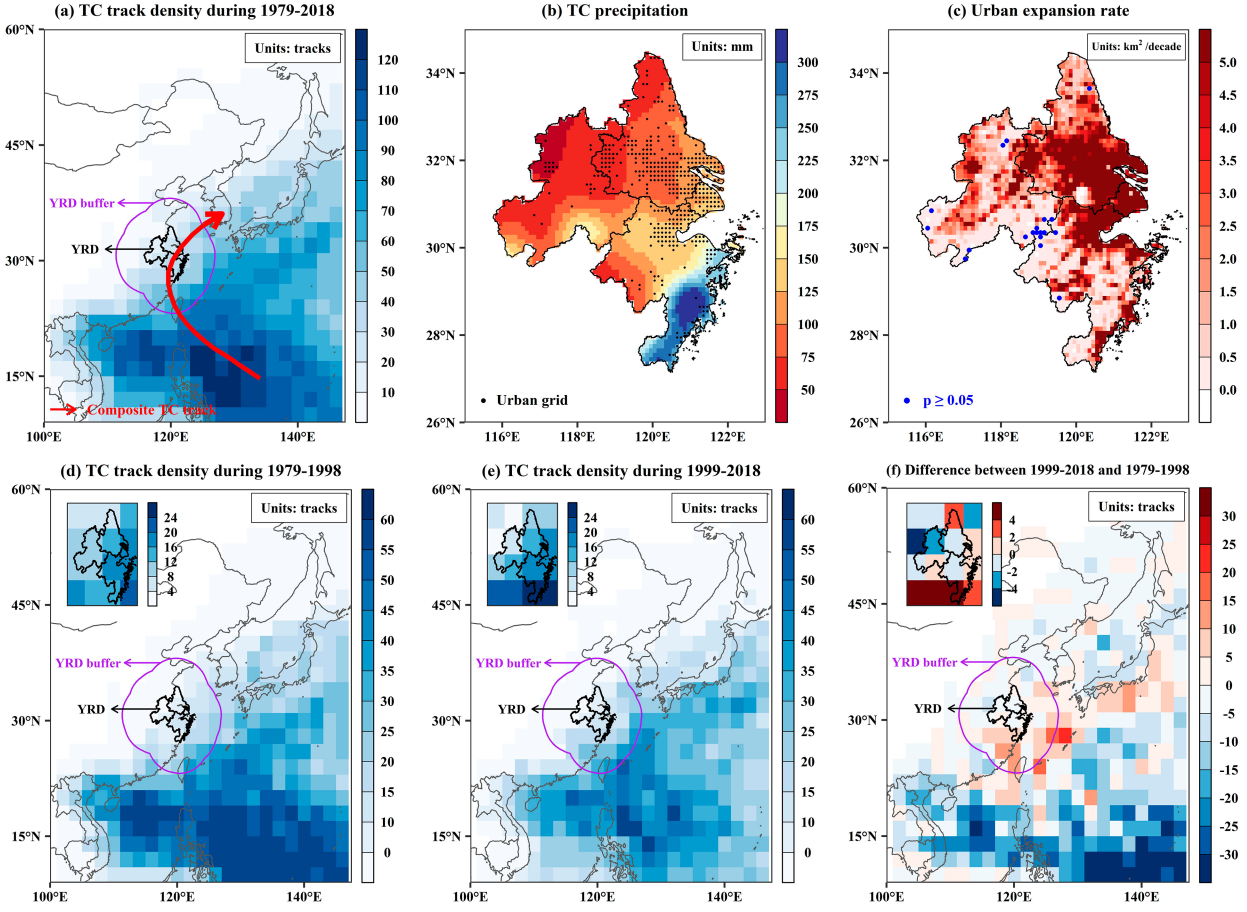

FIG. 1. (a) Spatial distribution of TC trajectories during 1979–2018 in the western North Pacific (WNP), (b) climatological means (1979–2018) of annual total TC-induced precipitation over the Yangtze River Delta (YRD) of eastern China, and (c) urbanization expansion rate during 1980–2015 over the YRD. (d)–(f) TC track density during two subperiods (i.e., 1979–98 and 1999–2018) and its difference between the two subperiods. In (a) and (d)–(f), the areas enclosed by the black (purple) line denote the YRD region (the 500-km YRD buffer), the color-filled areas show the accumulated frequency of TCs with a spatial resolution of 2° × 2°, and the red line marked with an arrow shows the composite track of 123 TCs crossing the 500-km YRD buffer. In (b), black dots represent urban grids, and the remaining grids represent rural grids. In (c), blue dots represent the grids where the urbanization expansion rate is not significant ($p \geq 0.05$); all other grids are significant.

We define two precipitation indices at the grid scale and at the event scale, respectively. For a given grid in the YRD region, all TC-induced precipitation events are identified every year. Taking one grid cell as an example (Fig. 2a), we identify seven TC-induced precipitation events in 2018. The accumulated TC-induced precipitation amounts (ATPA; units: mm) for each of the seven events are 4.2, 38.5, 16.9, 59.8, 43.6, 61.0, and 24.0 mm, respectively. Then, the annual-mean (maximum) ATPA of this grid in 2018 is computed as the average (maximum) value of these seven events, namely, 35.4 (61.0) mm.

For each TC-induced precipitation event, accumulated TC-induced precipitation volume (ATPV; units: km^3) is the sum of all 3-h precipitation volume during this event:

$$\text{ATPV} = p_1a_1 + p_2a_2 + \cdots + p_ka_k \ (i = 1, 2, \cdots, n), \quad (1)$$

where n represents the number of units of precipitation time (i.e., 3 h) caused by a TC; for each 3 h during a TC-induced precipitation event, $p_1, p_2, \ldots, p_k$ represent the area-weighted average precipitation depth for all grids affected by the TC, and $a_1, a_2, \ldots, a_k$ are the corresponding total areas of these grids.

Taking the precipitation event induced by Typhoon Jongdari in 2018 as an example, we plot the spatiotemporal evolution of this event every 3 h from 1 to 4 August over the YRD region (Fig. 2b). For each 3 h during this event, the precipitation volumes (i.e., area-weighted average of precipitation depth multiplied by the corresponding total area of TC-affected grids in every 3 h) are 0.0067, 0.1413, …, 0.1643, 0.0825, and 0.0135 km^3, respectively. The ATPV induced by Typhoon Jongdari is the sum of all these 3-h precipitation volumes, that is, 6.6163 km^3. Therefore, the annual-mean (maximum) ATPV is the average (maximum) value of all TC-induced precipitation events in a year.

c. *Quantification of urban effects on TC-induced precipitation*

Based on the LULC dataset developed by Xu et al. (2020), the urban area proportion in each grid point is calculated by

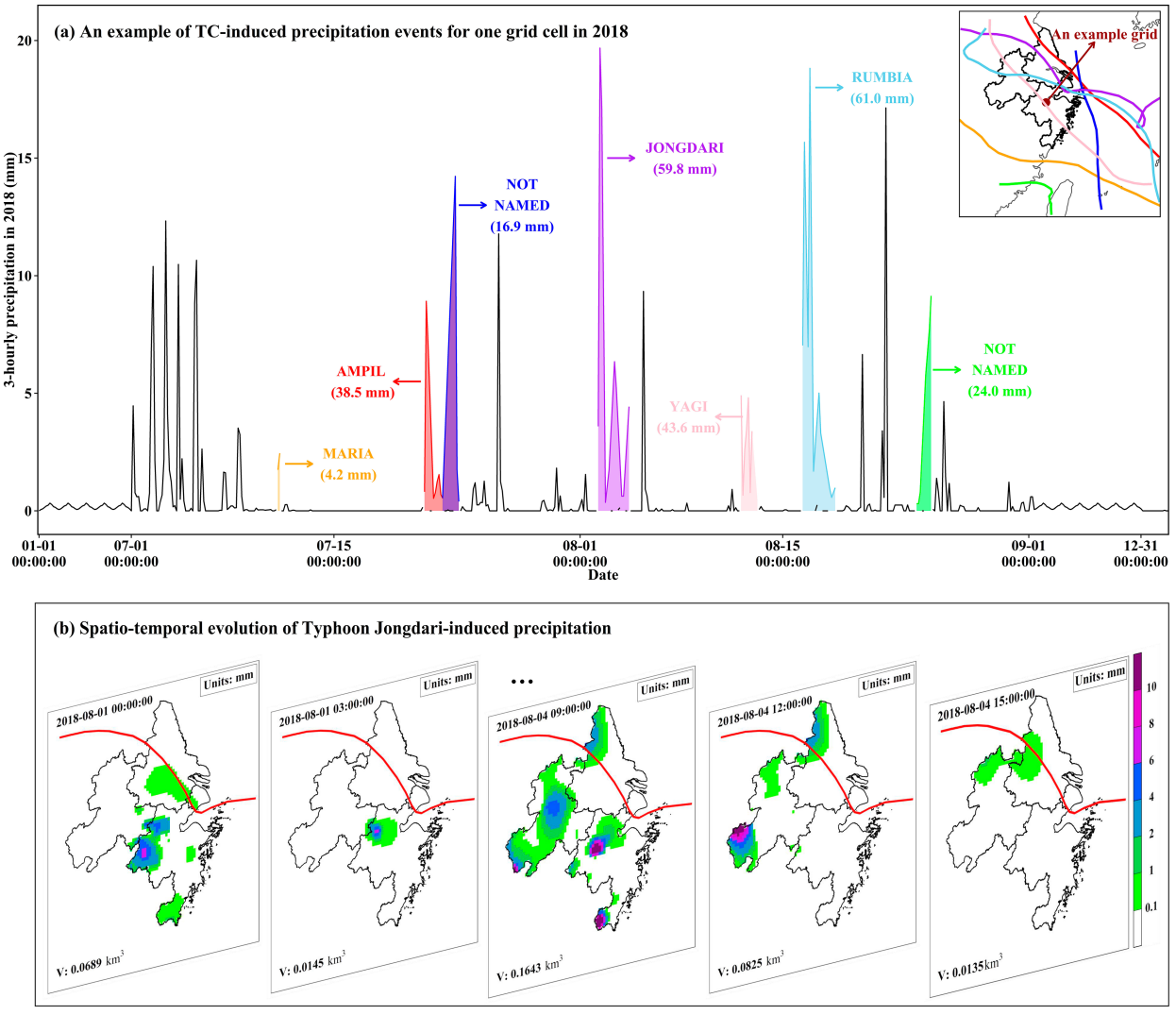

FIG. 2. Examples of TC-induced precipitation events. (a) This example grid cell experienced seven TC-induced precipitation events in 2018, including Typhoon Jongdari, which triggered a total of 59.8-mm precipitation in this grid. (b) Typhoon Jongdari reached the YRD region from 1 to 4 Aug 2018, and the spatial distribution of precipitation induced by Typhoon Jongdari at each 3 h is shown. The red line indicates the typhoon track over the entire period. The Jongdari-induced accumulated precipitation volume over the YRD region is 6.6163 km^3.

$(N_u/N_a) \times 100\%$, where N_u is the built-up area (i.e., urban area in this study) in a grid and N_a is the total area of this grid. The urbanization expansion rate (units: km^2 per decade) is defined as the rate of change in urban area for a given grid during 1980–2015 (Fig. 1c). Widespread urban sprawl is found in the YRD region, especially the central and eastern YRD. A grid is identified as an urban grid if the urban area proportion is greater than 35%. This percentage is consistent with previous studies (X. Yang et al. 2017; Luo and Lau 2019).

All the grids over YRD are divided into two categories: urban and rural grids. In section 3b, we define four indices to quantify TC-induced precipitation: annual-mean (maximum) ATPA and annual-mean (maximum) ATPV. Then, the four indices are calculated over urban grids as P_u and over rural grids as P_r. Calculating TC-induced precipitation in this way can ensure a minor difference in TC durations between urban and rural areas within TC-affected regions. With reference to previous studies on the effect of urbanization on surface air temperature (Luo and Lau 2019; Ren and Zhou 2014) and precipitation (Li et al. 2020, 2023; Yu et al. 2022), the urban effect and urban contribution metrics are adopted to quantify the impacts of urbanization on TC-induced precipitation. The urban effect is quantified as $|\text{Trend}\_P_u - \text{Trend}\_P_r|$, and the urban contribution is estimated as $|(\text{Trend}\_P_u - \text{Trend}\_P_r)/\text{Trend}\_P_u| \times 100\%$, where Trend_P_u (Trend_P_r) is the Sen's slope of P_u (P_r). The way to estimate urban effects has a potential assumption that each TC-induced precipitation event has the same climate background (such as circulation pattern) between urban and rural grids in this TC-induced precipitation field. We must acknowledge that it is a sample approach to estimate urban impacts on

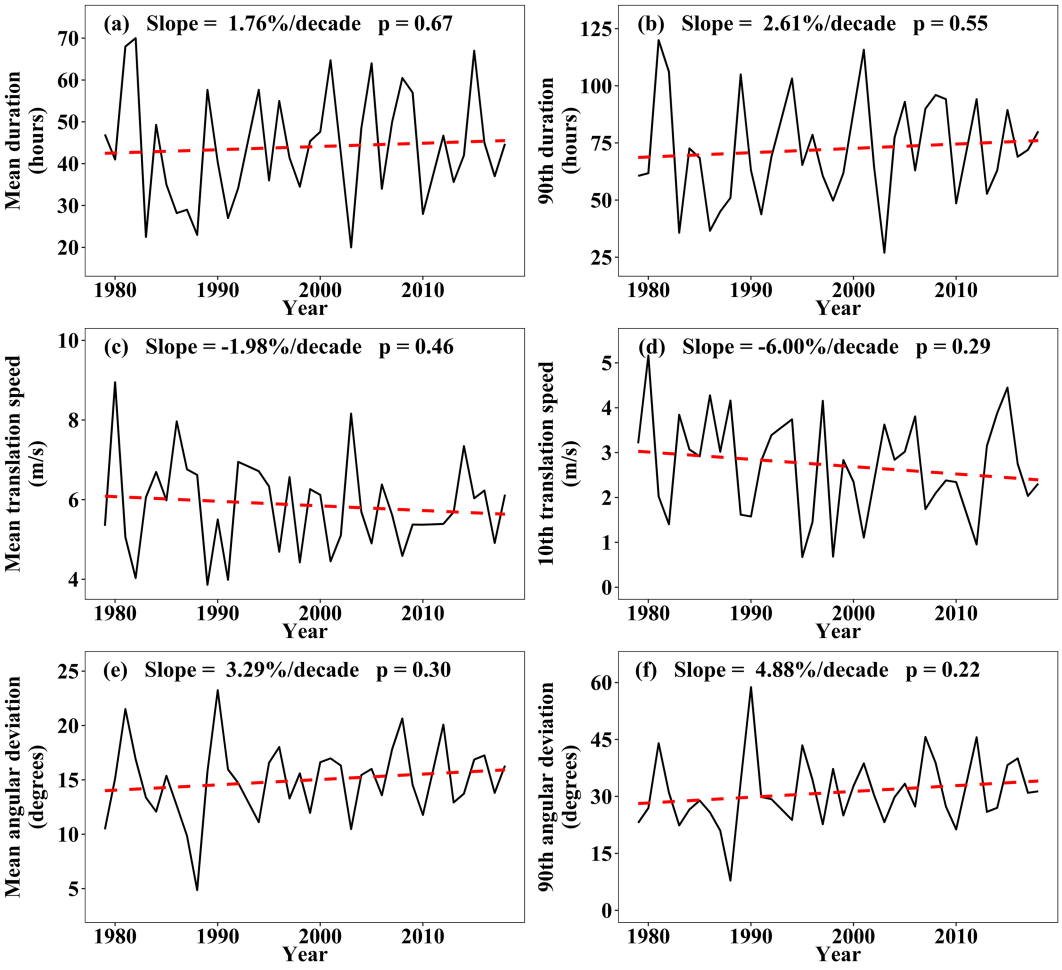

FIG. 3. Changes in TC (a),(b) duration, (c),(d) translation speed, and (e),(f) angular deviation within the 500-km YRD buffer during 1979–2018, where annual-mean duration and annual high duration (90th percentile of the annual values) are shown in (a) and (b), annual-mean translation speed and annual low translation speed (10th percentile of the annual values) are shown in (c) and (d), and annual-mean angular deviation and annual high angular deviation (90th percentile of the annual values) are shown in (e) and (f). The solid black line represents the original time series, and the dotted red line represents the fitted linear trend using the ordinary least squares method.

TC-induced precipitation without considering their complex interactions, such as nonlinear relationships.

The Sen's slope of P_u (P_r) in this study is estimated by the nonparametric modified Mann–Kendall method (Hamed and Rao 1998). The significance of differences in the Sen's slope of TC-induced precipitation between urban and rural areas (i.e., P_u and P_r) is estimated with a bootstrapping approach, similar to Vittal et al. (2013) and Singh et al. (2016). Specifically, we use the bootstrapping approach to subsampling time series from P_u (P_r) for 1000 times, and each subsampling time series has an equal length with original one. The nonparametric modified Mann–Kendall method is used to estimate Sen's slope of each subsampling time series. The Sen's slopes between P_u and P_r have an obvious difference if the two groups of their corresponding 1000 Sen's slopes from the 1000 subsampling time series are different at the 5% statistical significance level by the Student's t test.

4. Results

a. Variation characteristics of TC motions

Over the 500-km YRD buffer during 1979–2018, we observe a nonsignificant increasing trend in the annual-mean TC duration (1.76% per decade, $p = 0.67$; Fig. 3a), and this increasing trend is higher for longer-lasting TCs (90th percentile of annual TC duration: 2.61% per decade, $p = 0.55$; Fig. 3b), but still not significant. Chen et al. (2011) also found an upward trend in the overland duration of TCs over China during 1975–2009, and this national trend was significant. The increase in TC duration is directly related to the slower translation speed and increased angular deviation of TCs. Specifically, the annual-mean TC translation speed has decreased at a rate of −1.98% per decade ($p = 0.46$; Fig. 3c), and there is a faster decreasing rate for the slower-moving TCs (10th percentile of annual TC translation speed: −6.00% per decade, $p = 0.29$; Fig. 3d). This

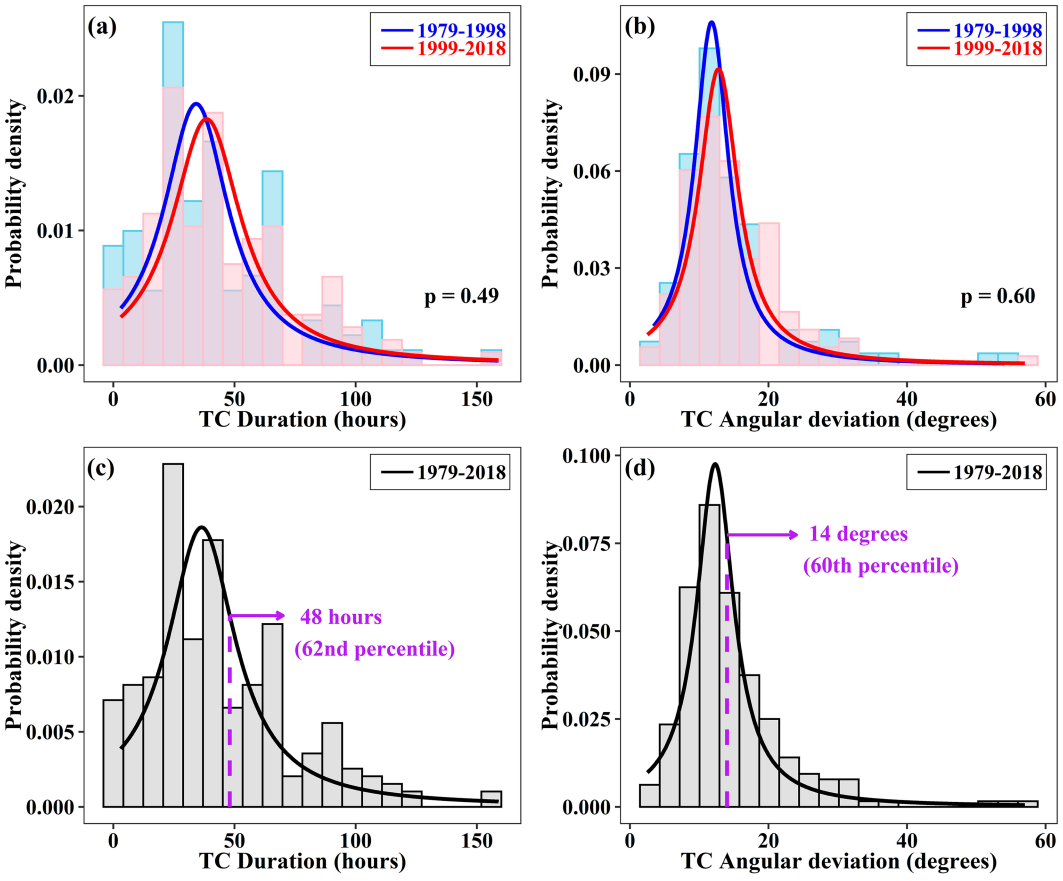

FIG. 4. Probability density functions (PDFs) of TC (a),(c) duration and (b),(d) angular deviation in the 500-km YRD buffer. PDFs of TC duration and angular deviation are shown during the periods of 1979–98 and 1999–2018 in (a) and (b) and in 1979–2018 in (c) and (d). The Kolmogorov–Smirnov test is used to test the difference between the two PDFs in (a) and (b) (see the p values).

result is consistent with Lai et al. (2020), who showed that TCs over the coastal areas of China have significantly slowed down during 1961–2017. In addition to the translation speed, we find an increasing tendency in the annual-mean TC angular deviation (3.29% per decade, $p = 0.30$; Fig. 3e), and this upward trend is faster for TCs with high angular deviation (90th percentile: 4.88% per decade, $p = 0.22$; Fig. 3f). Slow translation speed and large angular deviation can make TCs more likely to stall and meander in the 500-km YRD buffer, resulting in increased TC duration.

Each of the selected 123 TCs has a measured duration and angular deviation over the 500-km YRD buffer. Features of TC tracks over WNP, such as frequency, translation speed, and translation distance, have been reported with abrupt changes around the mid-1990s (W. Zhang et al. 2018; Lanzante 2019; Wang and Toumi 2021; Wang et al. 2023c). For example, W. Zhang et al. (2018) pointed out that the mean frequency of the WNP TCs was significantly reduced by 18% from the period 1980–96 to the period 1997–2014 (also see Figs. 1d–f in our study); Wang et al. (2023c) found an abrupt reduction in translation distance of the WNP TCs around the mid-1990s. Therefore, using these values from the selected 123 TCs in this study, we compare the probability density functions (PDFs) of individual TC duration and TC angular deviation between two periods of equal length (i.e., 1979–98 vs 1999–2018; Figs. 4a,b). Relative to the first half period, the PDFs of TC duration and angular deviation are both shifted to the right in the second half period, but the probability of TC duration and angular deviation reaching higher values is not significantly greater (TC duration: $p = 0.49$; TC angular deviation: $p = 0.60$) during 1999–2018 than during 1979–98. This confirms that TCs are becoming longer-lasting and increasingly wandering over the 500-km YRD buffer, increasing the probability of stalling TCs. We define stalling TCs using the PDFs of TC duration and angular deviation over the 500-km YRD buffer during 1979–2018 (Figs. 4c,d), consistent with the approach in Hall and Kossin (2019). In this study, a TC is identified as a stalling TC if its duration exceeds 48 h and its angular deviation is larger than 14 degrees (both above the 60th percentile value of the corresponding PDF).

Both the annual number of TCs with duration above 48 h and the annual fraction of above-48-h to total TCs show upward trends during 1979–2018 (i.e., 10.67% and 6.28% per decade, respectively; Figs. 5a,b). Additionally, the upward trend

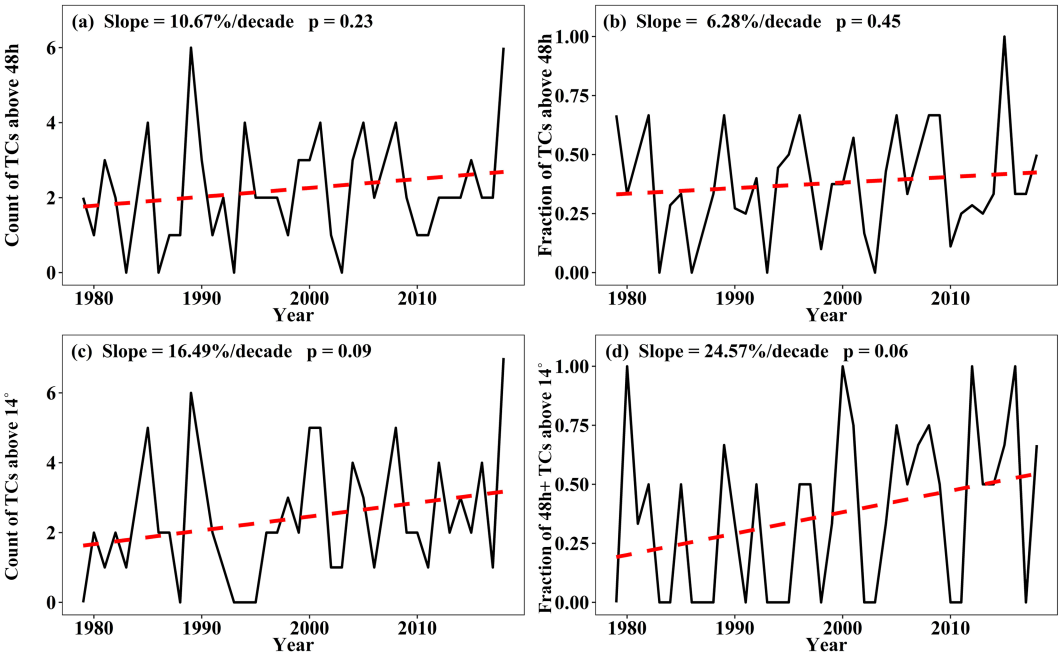

FIG. 5. Time series of annual number and proportion of stalling TCs over the 500-km YRD buffer during 1979–2018. The variables analyzed are (a) the annual number of TCs with duration exceeding 48 h, (b) annual proportion of above-48-h to total TCs, (c) annual number of TCs with angular deviation above 14°, and (d) annual proportion of stalling TCs (TC duration above 48 h and TC angular deviation above 14°). The solid black line represents the original time series, and the dotted red line represents the fitted linear trend using the ordinary least squares method.

is greater for the annual number of TCs with angular deviation above 14° (16.49% per decade; Fig. 5c). We notice that all the trend signals in the three characteristics of TC motions (Fig. 3) and the annual number or fraction of TCs with duration above 48 h (Figs. 5a,b) cannot pass the statistical significance test. These insignificant trends in the characteristics of TC motions (see Figs. 3 and 5) are likely affected by the short TC time series (1979–2018) where the trend signal is hard to distinguish from the noise due to the high natural variability of the TC itself. These results are similar to those of Hall and Kossin (2019), who found that the 1970s–2017 trends of TC translation speed and angular deviation over the North American coast have significance levels below 95%, less significant than trends of time series from 1944 to 2017. However, the fraction of stalling to total TCs has increased significantly during 1979–2018 (24.57% per decade, $p = 0.06$; Fig. 5d). TCs stall for a long time over the 500-km YRD buffer, implying that there is greater potential for severe torrential rainstorms and flooding.

The direct factors for the TC stalling are the slowing speed and wandering track of TC movement (Hall and Kossin 2019; Lai et al. 2020). Zhang et al. (2023) also found the stalling TCs over WNP and increasing TC-induced heavy precipitation over East Asian coast during 1979–2020. They pointed out that the TC stalling over WNP is associated with a significant trough anomaly to the northeast of TC location and that TC stalling is more likely affected by a second coexisting TC in the northeast. The binary cyclone interactions play an important role in triggering TC stalling over WNP (including our study region). Since TC stalling was found in recent years, the physical causes of TC stalling are poorly understood and should be further investigated in the future, which is beyond the scope of our study.

b. *Relations between TC-induced precipitation and TC duration*

TCs stalling over a region are expected to bring greater accumulated precipitation to the region. To validate this expectation, we further analyze the relationship between TC-induced precipitation and TC duration (Fig. 6). Quantile regression (Koenker and Bassett 1978) of ATPV by TC duration for the 123 TCs shows that ATPV increases with the increase in TC duration for all five quantiles (i.e., 5th, 25th, 50th, 75th, and 95th; $p < 0.01$ except for the 5th) and the positive dependence between ATPV and TC duration is stronger in higher quantiles (Fig. 6a). We bin the ATPV values of the 123 TCs into each category of TC duration, i.e., 0–12, 12–24, … , and 108–120 h (Fig. 6b). It can be seen that the longer the TC duration, the greater the ATPV (Fig. 6b). Hall and Kossin (2019) also found an obvious increase in ATPV per TC with residence time along the North American coast during 1948–2017.

Annual-mean and maximum ATPV and their linear trends are computed, respectively (Figs. 6c,d). The annual-mean (maximum) ATPV and annual-mean (high) TC duration fluctuate year to year in a relatively consistent manner (Figs. 6c,d), with both pairs showing significantly ($p < 0.05$) positive correlations (i.e., 0.64 and 0.58, respectively). This suggests that ATPV is strongly influenced by TC duration at the interannual scale.

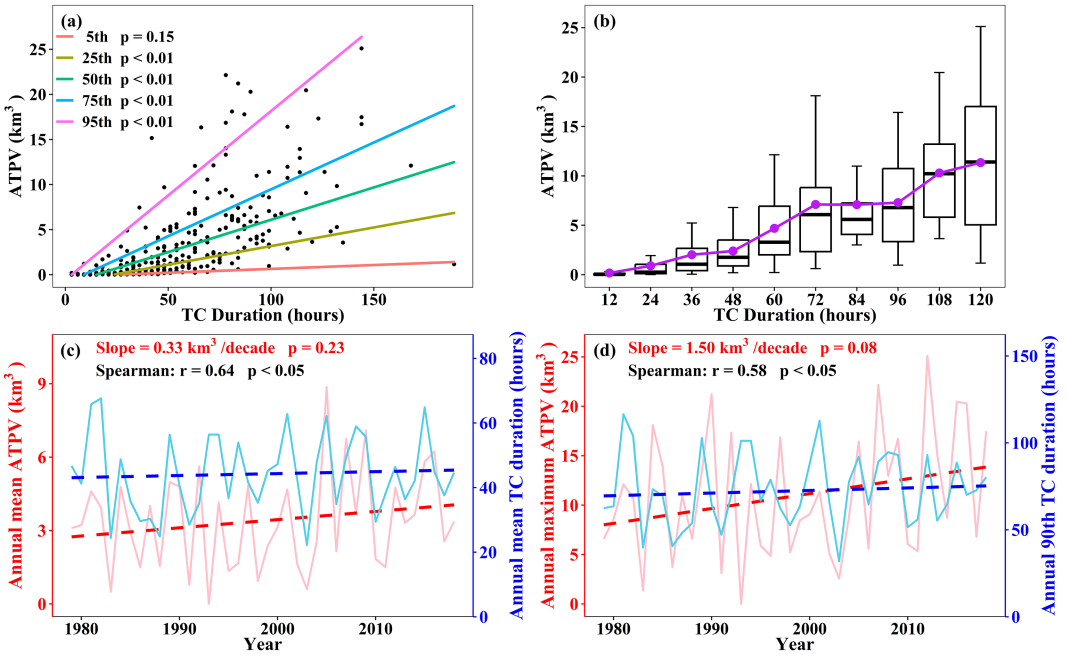

FIG. 6. (a)–(d) Relationships between accumulated TC-induced precipitation volume (ATPV) over the YRD region and TC duration over the 500-km YRD buffer during 1979–2018. In (a), each black dot denotes a TC-induced precipitation event, and this event is a function of TC duration and ATPV; the solid-colored lines are the 5th, 25th, 50th, 75th, and 95th quantile regressions of ATPV by TC duration, respectively. In (b), boxplots show ATPV of these events within each category of TC duration; the purple line indicates mean ATPV of the events within each category of TC duration. In (c), the blue (red) solid line is the time series of annual-mean TC duration (annual-mean ATPV); the blue (red) dashed line is the corresponding linear trend derived from the ordinary least squares method; and the correlation between annual-mean TC duration and annual-mean ATPV is estimated using the Spearman method. Finally, (d) is the same as (a), but for 90th percentile of annual TC durations and annual maximum ATPV.

Additionally, the annual-mean (maximum) ATPV has an upward trend of 0.33 (1.5) km^3 per decade.

For TC-induced precipitation events in each grid of the YRD region, annual-mean (maximum) ATPA and their linear trends are computed during 1979–2018 (Figs. 7a,b). The YRD region is dominated by increasing trends (at about 85% of grids) in both annual-mean and maximum ATPA, especially over the eastern and northwestern YRD. We calculate anomalies of annual-mean (maximum) ATPA for each grid and then average these anomalies regionally (Figs. 7e,f). Both the regional averages of annual-mean and maximum ATPA anomalies have a positive but weakly significant trend of 3.0 and 7.9 mm per decade, respectively. This positive trend in annual-mean (maximum) ATPA is consistent with but stronger than that in annual-mean (high) TC duration.

The correlation coefficients between annual-mean (maximum) ATPA and annual-mean (high) TC duration are significantly ($p < 0.05$) positive in the whole YRD region (Figs. 7c,d), suggesting that TC-induced precipitation at the grid scale is also strongly affected by TC duration at the interannual scale. Notably, the correlation coefficients between annual-mean (maximum) ATPA and annual-mean (high) TC duration are much lower in central and eastern YRD (Figs. 7c,d) where the urbanization expansion rate is the highest in the YRD region (Fig. 1c). This implies that urbanization could weaken the positive relationship between ATPA and TC duration; in other words, the duration of a TC over an urban area may not be the only factor explaining the total precipitation.

c. *Impacts of urban expansion on TC-induced precipitation*

As shown in Figs. 7c and 7d, TC-induced precipitation may potentially be influenced by urban expansion. To investigate the relationship between TC-induced precipitation and urban expansion, we bin trends in annual-mean (maximum) ATPA for all grids into each category of urbanization expansion rate (i.e., <0, 0–3, 3–6, …, and >21 km^2 per decade; Fig. 8). We find that trends in annual-mean (maximum) ATPA roughly increase with the urbanization expansion rate. However, this increase is not monotonous; that is, the relationship between changes in TC-induced precipitation and urbanization expansion rate is nonlinear. Yao et al. (2022) built nonstationary models to nonlinearly regress precipitation extremes by impervious areas over the YRD region and then quantify the urbanization effects. We further quantify the impacts of urbanization on changes in TC-induced precipitation (Fig. 9). To compute the two precipitation indices (annual-mean APTA and annual maximum APTA) at the grid scale, we first calculate the anomalies of annual-mean (maximum) ATPA relative to a climatological period of 1979–2018 for each grid of

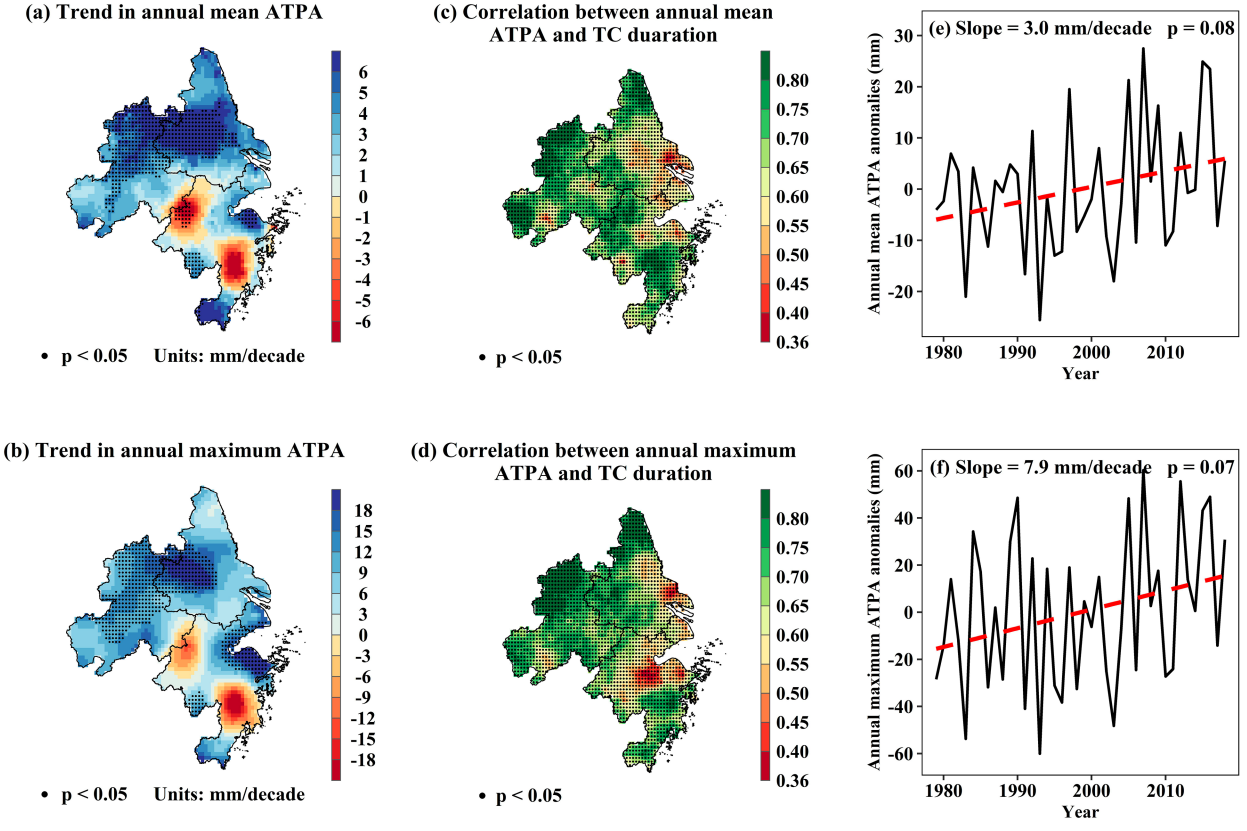

FIG. 7. Spatiotemporal changes of accumulated TC-induced precipitation amounts (ATPA) and their correlation with TC duration in the YRD during 1979–2018. (a) Spatial distribution of trend in annual-mean ATPA (black dots indicate trends at a 0.05 significance level). (c) Spatial distribution of Spearman correlation coefficient between annual-mean ATPA and TC duration (black dots indicate correlations at a 0.05 significance level). (e) The black line shows temporal change in regional average of annual-mean ATPA anomalies (computed relative to the climatological period 1979–2018); red dashed line is the corresponding linear trend derived from the ordinary least squares method. (b),(d),(f) As in (a), (c), and (e), respectively, but for annual maximum ATPV.

the YRD region and average the anomalies from all rural and urban grids, respectively (Figs. 9a,b). For the two precipitation indices at event scale (annual-mean ATPV and annual maximum ATPV), we calculate the ATPV of each TC over rural and urban areas, respectively, severally count the annual-mean (maximum) ATPV for corresponding areas, and extract their anomalies (Figs. 9c,d) by removing the climatological mean.

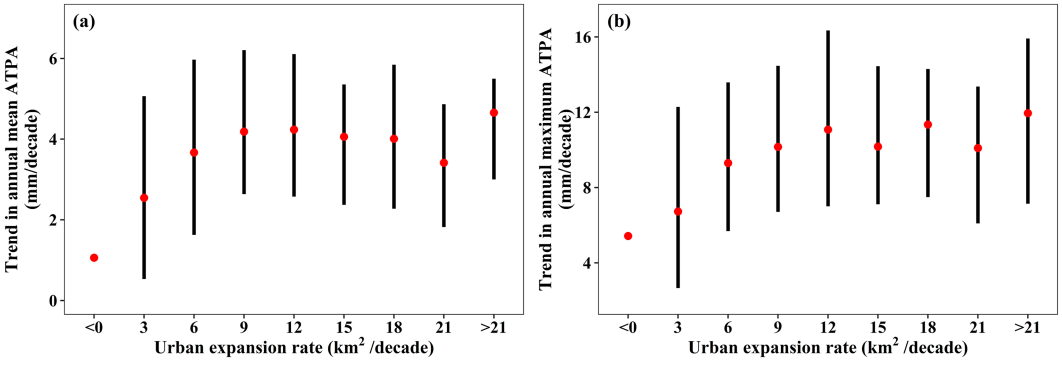

FIG. 8. (a),(b) The relationship between ATPA and urbanization expansion rate over the YRD region during 1979–2018. In (a), each matchstick indicates trends of annual-mean ATPA in grids within the corresponding category of urban expansion rate. The top and bottom of a matchstick represent the 75th and 25th percentiles of the distribution of trends, and the red dot represents the mean of corresponding rank. Note that (b) is the same as (a), but for annual maximum ATPA.

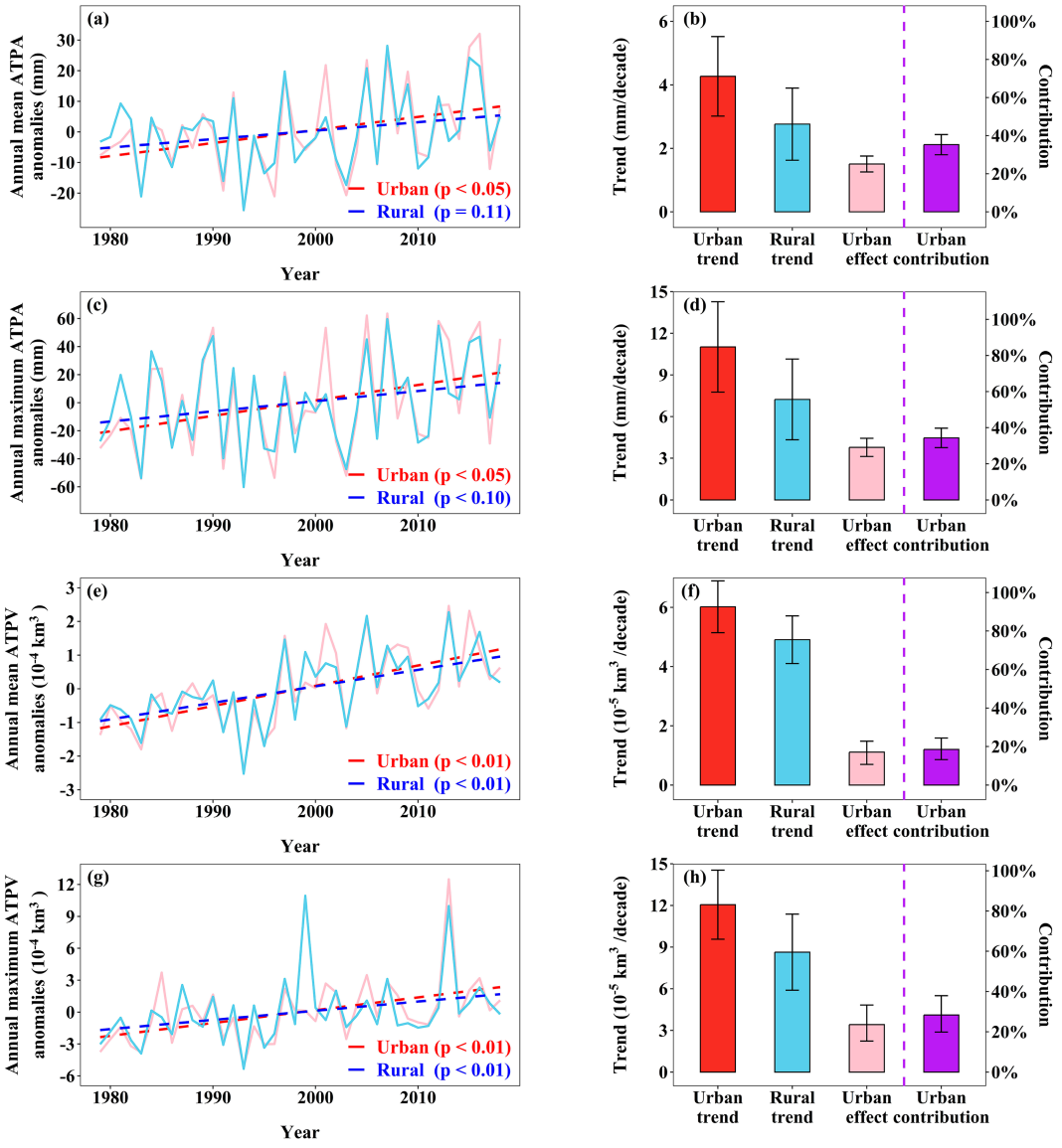

FIG. 9. Time series of regionally averaged anomalies in annual TC-induced precipitation for urban and rural areas over the YRD during 1979–2018. (a) Annual-mean ATPA anomalies from all rural (urban) grids are averaged year by year and then are shown as the blue (red) solid line; and the blue (red) dashed line is the corresponding linear trend derived from the ordinary least squares method. (b) Bar plots show linear trends corresponding to (a), and estimated urban effect and contribution. The other panels are the same as (a) and (b), but for (c),(d) annual maximum ATPA, (e),(f) annual-mean ATPV, and (g),(h) annual maximum ATPV. The differences of trends between urban and rural time series are all significant ($p < 0.05$) by the Student's t test (see section 3c).

In rural areas, the anomalies of annual-mean ATPA, annual maximum ATPA, annual-mean ATPV, and annual maximum ATPV all showed increasing trends of 2.8 mm per decade, 7.2 mm per decade, 4.9 $\times$ 10^{-5} km^3 per decade, and 8.6 $\times$ 10^{-5} km^3 per decade (Figs. 9a,c,e,g), respectively. However, these rising trends are greater in urban areas, with trends of 4.3 mm per decade, 11.0 mm per decade, 6.0 $\times$ 10^{-5} km^3 per decade, and 12.0 $\times$ 10^{-5} km^3 per decade, respectively. These significantly higher slopes (by the Student's t test) indicate that urbanization has enhanced TC-induced precipitation. Specifically, urban effects of annual-mean ATPA, annual maximum ATPA, annual-mean ATPV, and annual maximum ATPV are estimated as 1.5 mm per decade, 3.8 mm per decade, 1.1 $\times$ 10^{-5} km^3 per decade, and 3.4 $\times$ 10^{-5} km^3 per decade (Figs. 9b,d,f, and h), respectively. It is estimated that urbanization contributes 35.3%, 34.3%, 18.5%, and 28.4% of the increase in annual-mean ATPA, annual maximum ATPA, annual-mean ATPV, and annual maximum ATPV over the YRD urban areas.

In this study, a grid is identified as an urban grid if the urban area proportion is greater than 35%. We also test

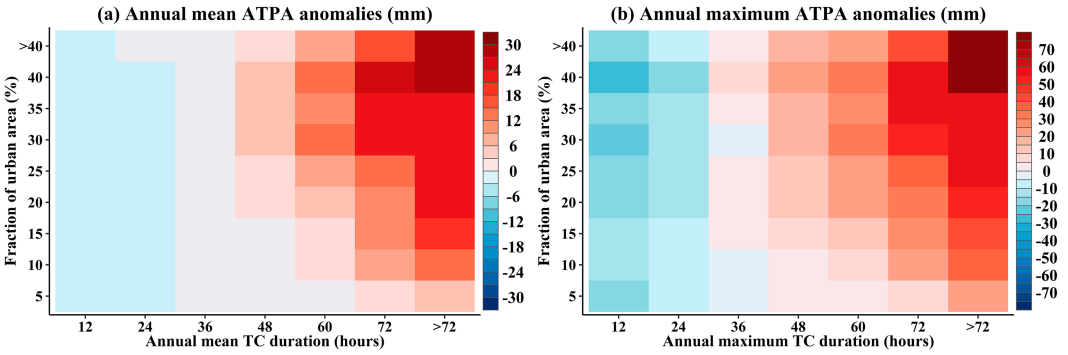

FIG. 10. Annual-mean (maximum) ATPA anomalies as a function of the annual-mean (maximum) TC duration and the fraction of urban area. In each grid in the YRD, the fraction of urban area is the percentage of built-up area to the total area of the given grid in 2015.

whether our results are sensitive to this proportion. When the urban area proportion is changed from 30% to 45% (i.e., 30%, 35%, 40%, and 45%), urban contributions to TC-induced precipitation are estimated as 18.5%–36.9%, 18.5%–35.3%, 18.5%–33.7%, and 18.5%–32.9%, respectively. These urban contributions show no obvious difference, suggesting that our analysis results are robust. The contribution values in our study are consistent with those shown in previous studies (Jiang et al. 2020; Han et al. 2022; Yu et al. 2022; Li et al. 2023) where urban impacts on heavy precipitation over the YRD urban areas were quantified. For example, over the YRD urban areas during 1961–2019, Li et al. (2023) estimated that urbanization contributed to the increases in frequency, duration, and intensity of heavy precipitation by 22.7%–37.5%, and Han et al. (2022) estimated this contribution to the increase in intensity of heavy precipitation as 24.8%. These consistent results enhance our confidence on the estimated contributions of urbanization to TC-induced precipitation. However, we must acknowledge that there are large uncertainties in these estimations using this sample approach. For example, one of the potential assumptions in this approach is that impacts of urbanization on long-term changes of TC-induced precipitation are linear, which may not be accurate (see the relationship between TC-induced precipitation and urbanization expansion rate over the YRD region in Fig. 8). Despite these uncertainties, the estimated contributions in our study can provide a valuable reference to the impacts of urbanization on long-term changes in TC-induced precipitation over urban areas. We also emphasize that numerical simulations should be developed to confirm the role of urbanization in the long-term changes of TC-induced precipitation in the future.

The correlations of the anomalies of annual-mean ATPA, annual maximum ATPA, annual-mean ATPV, and annual maximum ATPV between urban and rural areas are all statistically significant, with values being 0.90, 0.92, 0.93, and 0.78, respectively. These significant correlations are also shown in heavy precipitation (despite induced by TCs or not) between urban and rural areas of the YRD region (Yu et al. 2022; Han et al. 2022). These significant correlations suggest that variability of heavy precipitation at interannual or a larger scale is not determined by urbanization. For TC-induced heavy precipitation, its variability is mainly affected by TC tracks, which is confirmed by the significant correlations between annual-mean/maximum ATPA and TC duration (Figs. 7c,d). However, in this study, we analyze the impacts of urbanization on long-term trends in TC-induced precipitation, similar to Yu et al. (2022) and Han et al. (2022). Although the variability of TC-induced precipitation is dominated by TC tracks, urbanization can enhance the magnitude of TC-induced precipitation and hence lead to a faster increase in urban areas.

Since both TC duration and urban expansion influence TC-induced precipitation, we bin annual-mean (maximum) ATPA anomalies of all the YRD grids as a function of the annual-mean (maximum) TC duration and the fraction of urban area (Fig. 10). A positive association between annual-mean (maximum) ATPA anomalies and TC duration is evident, and this is the case between annual-mean (maximum) ATPA anomalies and the fraction of urban area. The highest annual-mean (maximum) ATPA anomalies occur in the grids with the longest-lasting TCs and with largest fraction of urban area. This suggests the increase in TC duration and rapid urbanization expansion have combined to amplify TC-induced precipitation over the urban areas of the YRD.

d. Possible mechanisms for the urbanization-enhanced TC-induced precipitation

The enhancing effects of urbanization on precipitation can be attributed to the UHI effect and changes in surface roughness (Miao et al. 2011; Zhong et al. 2015; Zhong and Yang 2015; Li et al. 2020; Q. Zhang et al. 2018). The UHI effect is a phenomenon where the air temperature in the city is significantly higher than in the surrounding areas. The warming surface perturbs the atmospheric boundary layer, destabilizes the atmospheric stratification, and yields heat island circulation. This effect can promote the formation of convective precipitation and intensify heavy rainfall, when there is sufficient water vapor, abundant condensation nuclei, or other favorable weather conditions (Li et al. 2020; Zhong and Yang 2015; Zhong et al. 2015). Additionally, the larger roughness of urban surfaces relative to the surroundings generates increased friction velocities, which can reduce near-surface wind speeds,

leading to the convergence of near-surface wind fields and triggering convective precipitation (Hu et al. 2018; Yang et al. 2018; Miao et al. 2011; W. Zhang et al. 2018). Meanwhile, the increased density and height of urban built structures can prolong the residence time of precipitation systems over the city, making precipitation longer-lasting and more intense (Zhang et al. 2019; Hu et al. 2018; Yue et al. 2019).

Whether the effects of UHIs and surface roughness can enhance TC-induced precipitation in urban areas has been investigated by numerical simulations of several TC events (Deng et al. 2022; W. Zhang et al. 2018; Ao et al. 2022; Du et al. 2023). The numerical simulations on precipitation induced by Typhoon Rumbia (2018) and Typhoon Lekima (2019) over the YRD region showed that the enhancement of surface sensible heat flux over urban areas is quite weak around the TC landfall time (Du et al. 2023; Ao et al. 2022). Their results suggested that the very weak UHI intensity before and during TC-induced precipitation is not the main reason for the enhancement of urbanization on TC-induced precipitation. However, the numerical simulations of precipitation induced by Hurricane Harvey (2017) in Houston in the United States indicated that the enhancement of Harvey-induced precipitation over urban areas can be partly explained by the UHI effects (e.g., changes in sensible heat flux and Bowen ratio; W. Zhang et al. 2018). This inconsistency on the role of UHI effects in previous studies may relate to uncertainties of single TC simulations and/or differences of background climate.

Nevertheless, previous studies have produced a consensus that atmospheric dynamic responses to increasing surface roughness play a key role in enhancing TC-induced precipitation over urban areas (Deng et al. 2022; W. Zhang et al. 2018; Ao et al. 2022; Du et al. 2023). Specifically, stronger friction velocity induced by larger surface roughness can slow the tangential wind, strengthen upward motion, increase water vapor mixing ratio, enhance low-level convergence and upper-level divergence, and finally lead to larger TC-induced precipitation rate in urban areas. Moreover, surface drag may also have a stalling effect on the TCs (Zhang et al. 2019; Hu et al. 2018; Yue et al. 2019), causing their precipitation systems to linger over the cities for longer, which in turn may enhance TC-induced precipitation. Since the simulation results on the urbanization effects from one single TC case have large uncertainties (Ao et al. 2022), the physical mechanisms (e.g., thermodynamic and dynamic responses) for impacts of urbanization on TC-induced precipitation should be deeply explored from a long-term perspective in the future.

5. Conclusions

The YRD region in eastern China is highly urbanized and frequently impacted by TCs. In this study, we find that TCs in the 500-km YRD buffer have become slower-moving, increasingly wandering, and longer-lasting during 1979–2018. In particular, the annual proportion of stalling TCs (with duration exceeding 48 h and angular deviation larger than 14°) to total TCs has significantly increased. Significant positive correlations between TC-induced precipitation and TC duration indicate the longer the TC duration, the greater the TC-induced precipitation. This positive association supports the finding that TCs stalling over the 500-km YRD buffer are more likely to expose the region to severe TC-induced precipitation. A consistent increasing trend is observed for both TC-induced precipitation and TC duration; however, the increase is higher for ATPV than for TC duration. Meanwhile, the significant positive correlation between TC-induced precipitation and TC duration across the YRD region is weaker in areas with high urban expansion rates. This difference suggests that other factors, such as urbanization, may also affect TC-induced precipitation.

We analyze the effects of urban expansion on TC-induced precipitation and find that the areas with higher urban expansion rates also show faster increases in TC-induced precipitation. Long-term increases in TC-induced precipitation over urban areas are markedly higher than over rural areas. By comparing the trends between urban and rural areas, we find that urbanization plays an important role in the long-term increases of TC-induced precipitation over urban areas. Taking the annual-mean (maximum) ATPA anomalies as a function of the annual-mean (maximum) TC duration and the fraction of urban area, we find that grid cells with a larger fraction of urban area and longer TC duration witness higher TC-induced precipitation, suggesting that both longer-lasting TCs and urban expansion amplify TC-induced precipitation.

Under global warming, climate models project that the reduction in both TC translation speed (Yamaguchi et al. 2020; Zhang et al. 2020) and in the decay of TC intensity after landfall (Li and Chakraborty 2020) will continue, likely leading to longer TC duration in the future. Meanwhile, urban areas are continuously expanding in the YRD region and other megalopolises of the world. Given the expansion of urban areas and possibly longer-lasting TCs, numerous cities are likely to be impacted by increasingly intense TC-induced precipitation. Our results suggest that adaptation measures should be adopted by urban managers to mitigate the storm hazards amplified by the combined effects of urbanization and TCs.

Acknowledgments. This work was financially supported by the China National Key R&D Program (Grant 2023YFF0807000), the National Natural Science Foundation of China (Grants U1911205, U2340230, 42371041, 42101052, and 41901041), the Key R&D Program of Hubei province, China (Grant 2023BCB117), the Guiding project of the Scientific Research Plan of the Education Department of Hubei Province (Grant B2022265), open funding from the Guangdong-Hong Kong Joint Laboratory for Water Security (Grant 2020B1212030005), and open funding from the State Key Laboratory of Water Resources and Hydropower Engineering Science (Wuhan University) (Grant 2021SWG01). Xihui Gu was supported by the China Scholarship Council. Louise Slater was supported by UKRI (MR/V022008/1) and NERC (NE/S015728/1). The authors declare that they have no competing interests.

Data availability statement. The tropical cyclone best track dataset is obtained from the International Best Track Archive

for Climate Stewardship Version 4.0 available at https://www.ncei.noaa.gov/products/international-best-track-archive?name=ib-v4-access. The China meteorological forcing dataset is collected from the National Tibetan Plateau Data Center available at https://data.tpdc.ac.cn/en/data/8028b944-daaa-4511-8769-965612652c49/. The land use/land cover data were developed by Xu et al. (2020) and are available at https://doi.org/10.5281/zenodo.3923728. All codes related to our results are available from the corresponding author (Xihui Gu) on reasonable request.

REFERENCES

Ao, X., C. Yue, X. Yang, L. Deng, and W. Huang, 2022: Urbanization effects on rainfall processes induced by landfalling Typhoon Lekima (2019) over the Shanghai metropolitan area. *J. Hydrometeor.*, **23**, 1075–1093, https://doi.org/10.1175/JHM-D-21-0170.1.

Chen, F., and Coauthors, 2020: Climate change, vegetation history, and landscape responses on the Tibetan Plateau during the Holocene: A comprehensive review. *Quat. Sci. Rev.*, **243**, 106444, https://doi.org/10.1016/j.quascirev.2020.106444.

Chen, X., L. Wu, and J. Zhang, 2011: Increasing duration of tropical cyclones over China. *Geophys. Res. Lett.*, **38**, L02708, https://doi.org/10.1029/2010GL046137.

Daloz, A. S., and S. J. Camargo, 2018: Is the poleward migration of tropical cyclone maximum intensity associated with a poleward migration of tropical cyclone genesis? *Climate Dyn.*, **50**, 705–715, https://doi.org/10.1007/s00382-017-3636-7.

Deng, Z., Z. Wang, X. Wu, C. Lai, and Z. Zeng, 2022: Strengthened tropical cyclones and higher flood risk under compound effect of climate change and urbanization across China's greater bay area. *Urban Climate*, **44**, 101224, https://doi.org/10.1016/j.uclim.2022.101224.

Du, X., H. Chen, Q. Li, and X. Ge, 2023: Urban impact on landfalling tropical cyclone precipitation: A numerical study of Typhoon Rumbia (2018). *Adv. Atmos. Sci.*, **40**, 988–1004, https://doi.org/10.1007/s00376-022-2100-8.

Gu, X., Q. Zhang, J. Li, V. P. Singh, and P. Sun, 2019: Impact of urbanization on nonstationarity of annual and seasonal precipitation extremes in China. *J. Hydrol.*, **575**, 638–655, https://doi.org/10.1016/j.jhydrol.2019.05.070.

Hall, T. M., and J. P. Kossin, 2019: Hurricane stalling along the North American coast and implications for rainfall. *npj Climate Atmos. Sci.*, **2**, 17, https://doi.org/10.1038/s41612-019-0074-8.

Hamed, K. H., and A. R. Rao, 1998: A modified Mann-Kendall trend test for autocorrelated data. *J. Hydrol.*, **204**, 182–196, https://doi.org/10.1016/S0022-1694(97)00125-X.

Han, L., L. Wang, H. Chen, Y. Xu, F. Sun, K. Reed, X. Deng, and W. Li, 2022: Impacts of long-term urbanization on summer rainfall climatology in Yangtze River Delta agglomeration of China. *Geophys. Res. Lett.*, **49**, e2021GL097546, https://doi.org/10.1029/2021GL097546.

He, J., K. Yang, W. Tang, H. Lu, J. Qin, Y. Chen, and X. Li, 2020: The first high-resolution meteorological forcing dataset for land process studies over China. *Sci. Data*, **7**, 25, https://doi.org/10.1038/s41597-020-0369-y.

He, Q., J. Yang, H. Chen, J. Liu, Q. Ji, Y. Wang, and F. Tang, 2021: Evaluation of extreme precipitation based on three long-term gridded products over the Qinghai-Tibet Plateau. *Remote Sens.*, **13**, 3010, https://doi.org/10.3390/rs13153010.

Hu, Q., J. Zhang, Y. Wang, Y. Huang, Y. Liu, and L. Li, 2018: A review of urbanization impact on precipitation. *Adv. Water Sci.*, **29**, 138–150, https://doi.org/10.14042/j.cnki.32.1309.2018.01.016.

Jiang, H., and E. J. Zipser, 2010: Contribution of tropical cyclones to the global precipitation from eight seasons of TRMM data: Regional, seasonal, and interannual variations. *J. Climate*, **23**, 1526–1543, https://doi.org/10.1175/2009JCLI3303.1.

Jiang, X., Y. Luo, D.-L. Zhang, and M. Wu, 2020: Urbanization enhanced summertime extreme hourly precipitation over the Yangtze River Delta. *J. Climate*, **33**, 5809–5826, https://doi.org/10.1175/JCLI-D-19-0884.1.

Kang, N.-Y., and J. B. Elsner, 2012: Consensus on climate trends in western North Pacific tropical cyclones. *J. Climate*, **25**, 7564–7573, https://doi.org/10.1175/JCLI-D-11-00735.1.

Khouakhi, A., G. Villarini, and G. A. Vecchi, 2017: Contribution of tropical cyclones to rainfall at the global scale. *J. Climate*, **30**, 359–372, https://doi.org/10.1175/JCLI-D-16-0298.1.

Knapp, K. R., M. C. Kruk, D. H. Levinson, H. J. Diamond, and C. J. Neumann, 2010: The International Best Track Archive for Climate Stewardship (IBTrACS) unifying tropical cyclone data. *Bull. Amer. Meteor. Soc.*, **91**, 363–376, https://doi.org/10.1175/2009BAMS2755.1.

Knight, D. B., and R. E. Davis, 2009: Contribution of tropical cyclones to extreme rainfall events in the southeastern United States. *J. Geophys. Res.*, **114**, D23102, https://doi.org/10.1029/2009JD012511.

Koenker, R., and G. Bassett Jr., 1978: Regression quantiles. *Econometrica*, **46**, 33–50, https://doi.org/10.2307/1913643.

Kossin, J. P., 2018: A global slowdown of tropical-cyclone translation speed. *Nature*, **558**, 104–107, https://doi.org/10.1038/s41586-018-0158-3.

——, 2019: Reply to: Moon, I.-J. et al.; Lanzante, J. R. *Nature*, **570**, E16–E22, https://doi.org/10.1038/s41586-019-1224-1.

——, T. L. Olander, and K. R. Knapp, 2013: Trend analysis with a new global record of tropical cyclone intensity. *J. Climate*, **26**, 9960–9976, https://doi.org/10.1175/JCLI-D-13-00262.1.

Lai, Y., and Coauthors, 2020: Greater flood risks in response to slowdown of tropical cyclones over the coast of China. *Proc. Natl. Acad. Sci. USA*, **117**, 14 751–14 755, https://doi.org/10.1073/pnas.1918987117.

——, J. Li, X. Gu, C. Liu, and Y. D. Chen, 2021: Global compound floods from precipitation and storm surge: Hazards and the roles of cyclones. *J. Climate*, **34**, 8319–8339, https://doi.org/10.1175/JCLI-D-21-0050.1.

Landsea, C. W., B. A. Harper, K. Hoarau, and J. A. Knaff, 2006: Can we detect trends in extreme tropical cyclones? *Science*, **313**, 452–454, https://doi.org/10.1126/science.1128448.

——, G. A. Vecchi, L. Bengtsson, and T. R. Knutson, 2010: Impact of duration thresholds on Atlantic tropical cyclone counts. *J. Climate*, **23**, 2508–2519, https://doi.org/10.1175/2009JCLI3034.1.

Lanzante, J. R., 2019: Uncertainties in tropical-cyclone translation speed. *Nature*, **570**, E6–E15, https://doi.org/10.1038/s41586-019-1223-2.

Li, C., X. Gu, L. J. Slater, J. Liu, J. Li, X. Zhang, and D. Kong, 2023: Urbanization-induced increases in heavy precipitation are magnified by moist heatwaves in an urban agglomeration of East China. *J. Climate*, **36**, 693–709, https://doi.org/10.1175/JCLI-D-22-0223.1.

Li, L., and P. Chakraborty, 2020: Slower decay of landfalling hurricanes in a warming world. *Nature*, **587**, 230–234, https://doi.org/10.1038/s41586-020-2867-7.

Li, Y., and Coauthors, 2020: Strong intensification of hourly rainfall extremes by urbanization. *Geophys. Res. Lett.*, **47**, e2020GL088758, https://doi.org/10.1029/2020GL088758.

Liu, L., and Y. Wang, 2020: Trends in landfalling tropical cyclone-induced precipitation over China. *J. Climate*, **33**, 2223–2235, https://doi.org/10.1175/JCLI-D-19-0693.1.

Luo, M., and N.-C. Lau, 2019: Urban expansion and drying climate in an urban agglomeration of East China. *Geophys. Res. Lett.*, **46**, 6868–6877, https://doi.org/10.1029/2019GL082736.

Marsooli, R., N. Lin, K. Emanuel, and K. Feng, 2019: Climate change exacerbates hurricane flood hazards along US Atlantic and Gulf Coasts in spatially varying patterns. *Nat. Commun.*, **10**, 3785, https://doi.org/10.1038/s41467-019-11755-z.

Miao, S., F. Chen, Q. Li, and S. Fan, 2011: Impacts of urban processes and urbanization on summer precipitation: A case study of heavy rainfall in Beijing on 1 August 2006. *J. Appl. Meteor. Climatol.*, **50**, 806–825, https://doi.org/10.1175/2010JAMC2513.1.

Peduzzi, P., B. Chatenoux, H. Dao, A. De Bono, C. Herold, J. Kossin, F. Mouton, and O. Nordbeck, 2012: Global trends in tropical cyclone risk. *Nat. Climate Change*, **2**, 289–294, https://doi.org/10.1038/nclimate1410.

Qian, Y., and Coauthors, 2022: Urbanization impact on regional climate and extreme weather: Current understanding, uncertainties, and future research directions. *Adv. Atmos. Sci.*, **39**, 819–860, https://doi.org/10.1007/s00376-021-1371-9.

Ren, F., G. Wu, W. Dong, X. Wang, Y. Wang, W. Ai, and W. Li, 2006: Changes in tropical cyclone precipitation over China. *Geophys. Res. Lett.*, **33**, L20702, https://doi.org/10.1029/2006GL027951.

——, Y. Wang, X. Wang, and W. Li, 2007: Estimating tropical cyclone precipitation from station observations. *Adv. Atmos. Sci.*, **24**, 700–711, https://doi.org/10.1007/s00376-007-0700-y.

Ren, G., and Y. Zhou, 2014: Urbanization effect on trends of extreme temperature indices of national stations over mainland China, 1961–2008. *J. Climate*, **27**, 2340–2360, https://doi.org/10.1175/JCLI-D-13-00393.1.

Ren, M., Z. Xu, B. Pang, W. Liu, J. Liu, L. Du, and R. Wang, 2018: Assessment of satellite-derived precipitation products for the Beijing region. *Remote Sens.*, **10**, 1914, https://doi.org/10.3390/rs10121914.

Ress, L. D., C.-L. J. Hung, and L. A. James, 2020: Impacts of urban drainage systems on stormwater hydrology: Rocky Branch Watershed, Columbia, South Carolina. *J. Flood Risk Manage.*, **13**, e12643, https://doi.org/10.1111/jfr3.12643.

Shao, X., X. Jin, T. Luo, and K. Wei, 2021: Analysis of Super Typhoon Lekima flood and flood regulation in Zhejiang province. *Chin. J. Hydrol.*, **41**, 69–73, https://doi.org/10.19797/j.cnki.1000-0852.20200187.

Shao, Z., H. Fu, D. Li, O. Altan, and T. Cheng, 2019: Remote sensing monitoring of multi-scale watersheds impermeability for urban hydrological evaluation. *Remote Sens. Environ.*, **232**, 111338, https://doi.org/10.1016/j.rse.2019.111338.

Singh, J., H. Vittal, S. Karmakar, S. Ghosh, and D. Niyogi, 2016: Urbanization causes nonstationarity in Indian summer monsoon rainfall extremes. *Geophys. Res. Lett.*, **43**, 11 269–11 277, https://doi.org/10.1002/2016GL071238.

Song, J., P. J. Klotzbach, H. Zhao, and Y. Duan, 2021: Slowdown in the decay of western North Pacific tropical cyclones making landfall on the Asian continent. *Front. Earth Sci.*, **9**, 749287, https://doi.org/10.3389/feart.2021.749287.

Su, L., J. Li, X. Shi, and J. C. H. Fung, 2019: Spatiotemporal variation in presummer precipitation over south China from 1979 to 2015 and its relationship with urbanization. *J. Geophys. Res. Atmos.*, **124**, 6737–6749, https://doi.org/10.1029/2019JD030751.

Vittal, H., S. Karmakar, and S. Ghosh, 2013: Diametric changes in trends and patterns of extreme rainfall over India from pre-1950 to post-1950. *Geophys. Res. Lett.*, **40**, 3253–3258, https://doi.org/10.1002/grl.50631.

Wang, B., Y. Ma, Z. Su, Y. Wang, and W. Ma, 2020: Quantifying the evaporation amounts of 75 high-elevation large dimictic lakes on the Tibetan Plateau. *Sci. Adv.*, **6**, eaay8558, https://doi.org/10.1126/sciadv.aay8558.

Wang, J., J. Feng, and Z. Yan, 2018: Impact of extensive urbanization on summertime rainfall in the Beijing region and the role of local precipitation recycling. *J. Geophys. Res. Atmos.*, **123**, 3323–3340, https://doi.org/10.1002/2017JD027725.

Wang, L., X. Gu, and H. E. Beck, 2021: Cyclones and global floods from an observation-simulation evaluation: Contributions and long-term changes. *Water*, **13**, 2965, https://doi.org/10.3390/w13212965.

——, and Coauthors, 2022: An analysis of translation distance of tropical cyclones over the western North Pacific. *J. Climate*, **35**, 7643–7660, https://doi.org/10.1175/JCLI-D-22-0030.1.

——, X. Gu, L. J. Slater, Y. Lai, X. Zhang, D. Kong, J. Liu, and J. Li, 2023a: Indirect and direct impacts of Typhoon In-Fa (2021) on heavy precipitation in inland and coastal areas of China: Synoptic-scale environments and return period analysis. *Mon. Wea. Rev.*, **151**, 2377–2395, https://doi.org/10.1175/MWR-D-22-0241.1.

——, and Coauthors, 2023b: Attribution of the record-breaking extreme precipitation events in July 2021 over central and eastern China to anthropogenic climate change. *Earth's Future*, **11**, e2023EF003613, https://doi.org/10.1029/2023EF003613.

——, X. Gu, L. J. Slater, J. Li, D. Kong, X. Zhang, and J. Liu, 2023c: Phase shifts of the PDO and AMO alter the translation distance of global tropical cyclones. *Earth's Future*, **11**, e2022EF003079, https://doi.org/10.1029/2022EF003079.

Wang, S., and R. Toumi, 2021: Recent migration of tropical cyclones toward coasts. *Science*, **371**, 514–517, https://doi.org/10.1126/science.abb9038.

——, and Coauthors, 2020: Changes of water clarity in large lakes and reservoirs across China observed from long-term MODIS. *Remote Sens. Environ.*, **247**, 111949, https://doi.org/10.1016/j.rse.2020.111949.

Woodruff, J. D., J. L. Irish, and S. J. Camargo, 2013: Coastal flooding by tropical cyclones and sea-level rise. *Nature*, **504**, 44–52, https://doi.org/10.1038/nature12855.

Xu, H., and B. Du, 2015: The impact of Typhoon Danas (2013) on the torrential rainfall associated with Typhoon Fitow (2013) in East China. *Adv. Meteor.*, **2015**, 383712, https://doi.org/10.1155/2015/383712.

——, X. Zhang, and X. Xu, 2013: Impact of tropical storm Bopha on the intensity change of super Typhoon Saomai in the 2006 typhoon season. *Adv. Meteor.*, **2013**, 487010, https://doi.org/10.1155/2013/487010.

Xu, Y., and Coauthors, 2020: Annual 30-m land use/land cover maps of China for 1980–2015 from the integration of AVHRR, MODIS and Landsat data using the BFAST algorithm. *Sci. China Earth Sci.*, **63**, 1390–1407, https://doi.org/10.1007/s11430-019-9606-4.

Yamaguchi, M., J. C. L. Chan, I.-J. Moon, K. Yoshida, and R. Mizuta, 2020: Global warming changes tropical cyclone translation speed. *Nat. Commun.*, **11**, 47, https://doi.org/10.1038/s41467-019-13902-y.

Yang, H., 2019: Research on the climate characteristics of tropical cyclone precipitation in China from 1960 to 2017. M.S. thesis, State Key Laboratory on Severe Weather, Chinese Academy of Meteorological Sciences, 12 pp.

Yang, K., and J. He, 2019: China meteorological forcing dataset (1979–2018). National Tibetan Plateau Data Center, accessed 15 December 2022, https://doi.org/10.11888/AtmosphericPhysics.tpe.249369.file.

——, ——, W. Tang, J. Qin, and C. C. K. Cheng, 2010: On downward shortwave and longwave radiations over high altitude regions: Observation and modeling in the Tibetan Plateau. *Agric. For. Meteor.*, **150**, 38–46, https://doi.org/10.1016/j.agrformet.2009.08.004.

Yang, P., G. Ren, and P. Yan, 2017: Evidence for a strong association of short-duration intense rainfall with urbanization in the Beijing urban area. *J. Climate*, **30**, 5851–5870, https://doi.org/10.1175/JCLI-D-16-0671.1.

Yang, T., Y. Duan, J. Xu, and J. Feng, 2018: Simulation of the urbanization impact on precipitation of landfalling Tropical Cyclone Nida (2016). *J. Appl. Meteor. Sci.*, **29**, 410–422, https://doi.org/10.11898/1001-7313.20180403.

Yang, X., L. Ruby Leung, N. Zhao, C. Zhao, Y. Qian, K. Hu, X. Liu, and B. Chen, 2017: Contribution of urbanization to the increase of extreme heat events in an urban agglomeration in East China. *Geophys. Res. Lett.*, **44**, 6940–6950, https://doi.org/10.1002/2017GL074084.

Yao, R., S. Zhang, P. Sun, Q. Dai, and Q. Yang, 2022: Estimating the impact of urbanization on non-stationary models of extreme precipitation events in the Yangtze River Delta metropolitan region. *Wea. Climate Extremes*, **36**, 100445, https://doi.org/10.1016/j.wace.2022.100445.

Yu, X., and Coauthors, 2022: Asymmetrical shift toward less light and more heavy precipitation in an urban agglomeration of East China: Intensification by urbanization. *Geophys. Res. Lett.*, **49**, e2021GL097046, https://doi.org/10.1029/2021GL097046.

Yue, C., Y. Tang, W. Gu, Z. Han, and X. Wang, 2019: Study of urban barrier effect on local typhoon precipitation. *Meteor. Mon.*, **45**, 1611–1620, https://doi.org/10.7519/j.issn.1000-0526.2019.11.011.

Zhang, D.-L., M. S. Jin, Y. Shou, and C. Dong, 2019: The influences of urban building complexes on the ambient flows over the Washington–Reston region. *J. Appl. Meteor. Climatol.*, **58**, 1325–1336, https://doi.org/10.1175/JAMC-D-19-0037.1.

Zhang, G., H. Murakami, T. R. Knutson, R. Mizuta, and K. Yoshida, 2020: Tropical cyclone motion in a changing climate. *Sci. Adv.*, **6**, eaaz7610, https://doi.org/10.1126/sciadv.aaz7610.

Zhang, L., T. F. Cheng, M. Lu, R. Xiong, and J. Gan, 2023: Tropical cyclone stalling shifts northward and brings increasing flood risks to East Asian coast. *Geophys. Res. Lett.*, **50**, e2022GL102509, https://doi.org/10.1029/2022GL102509.

Zhang, Q., X. Gu, J. Li, P. Shi, and V. P. Singh, 2018: The impact of tropical cyclones on extreme precipitation over coastal and inland areas of China and its association to ENSO. *J. Climate*, **31**, 1865–1880, https://doi.org/10.1175/JCLI-D-17-0474.1.

Zhang, W., G. Villarini, G. A. Vecchi, and J. A. Smith, 2018: Urbanization exacerbated the rainfall and flooding caused by Hurricane Harvey in Houston. *Nature*, **563**, 384–388, https://doi.org/10.1038/s41586-018-0676-z.

Zhong, S., and X.-Q. Yang, 2015: Ensemble simulations of the urban effect on a summer rainfall event in the greater Beijing metropolitan area. *Atmos. Res.*, **153**, 318–334, https://doi.org/10.1016/j.atmosres.2014.09.005.

——, Y. Qian, C. Zhao, R. Leung, and X.-Q. Yang, 2015: A case study of urbanization impact on summer precipitation in the greater Beijing metropolitan area: Urban heat island versus aerosol effects. *J. Geophys. Res. Atmos.*, **120**, 10 903–10 914, https://doi.org/10.1002/2015JD023753.

Zhou, C., and Coauthors, 2022: The impact of Typhoon Lekima (2019) on East China: A postevent survey in Wenzhou City and Taizhou City. *Front. Earth Sci.*, **16**, 109–120, https://doi.org/10.1007/s11707-020-0856-7.

Zhou, F., Y. Xu, Y. Chen, C.-Y. Xu, Y. Gao, and J. Du, 2013: Hydrological response to urbanization at different spatio-temporal scales simulated by coupling of CLUE-S and the SWAT model in the Yangtze River Delta region. *J. Hydrol.*, **485**, 113–125, https://doi.org/10.1016/j.jhydrol.2012.12.040.

Zhu, Y.-J., and J. M. Collins, 2021: Recent rebounding of the post-landfall hurricane wind decay period over the continental United States. *Geophys. Res. Lett.*, **48**, e2020GL092072, https://doi.org/10.1029/2020GL092072.